

# Supporting Information for ”Heat-blanketed convection and its implications for the continental lithosphere”

K. Vilella<sup>1,2</sup>and F. Deschamps<sup>1</sup>

<sup>1</sup>Institute of Earth Sciences, Academia Sinica, Taipei, Taiwan

<sup>2</sup>JSPS International Research Fellow, Hokkaido University, Japan

## Contents of this file

1. Texts S1 to S3
2. Tables S1 and S2
3. Figures S1 to S4

## Text S1: Definition of the thermal boundary layer

A Thermal Boundary Layer (TBL) is generally assumed to be a layer close to an interface characterized by a large change of temperature and where heat is mainly transferred by conduction to the outside of the system. In practice, defining a TBL is highly subjective and authors have proposed many different methods leading to different results. Here, we will propose a brief overview of these methods and show how it affects the measured value of the temperature jump across the TBL ( $\Delta T_{TBL}$ ) and the thickness of the TBL

---

Corresponding author: K. Vilella (kennyvilella@gmail.com)

( $\delta_{TBL}$ ). Building on this discussion, we will describe the method used in this paper and the reasons behind this choice. Note that the discussion will only concern the top TBL.

Most authors define the TBL using the horizontally averaged temperature profile, which has the important characteristic of setting the amount of heat transferred by the system. Using this profile, the base of the TBL has been defined by a varieties of criteria, including the local maximum of temperature (e.g. Parmentier & Sotin, 2000), the point where the amount of heat transported by advection equals the amount of heat transported by conduction (e.g. Sotin & Labrosse, 1999), or where conduction is negligible (for instance, Vilella & Deschamps, 2018, defined the base of the TBL where the spatial derivative of temperature reaches 1% of its minimum value). For the sake of example, we report in figure S1 the measured value of  $\Delta T_{TBL}$  and  $\delta_{TBL}$  for the case where  $Ra = 10^6$  and  $H = 20$  and defining the TBL as either the maximum temperature or the point where conduction is negligible. First, we can see that the measured value of  $\Delta T_{TBL}$  is hardly affected by the criteria used to define the TBL. Moreover, the temporal fluctuations of  $\Delta T_{TBL}$ , represented by the error bars, are also negligible. By contrast,  $\delta_{TBL}$  is subject to significant deviations following the definition used and also subject to important temporal fluctuations. As a general rule, one should consider the value of  $\Delta T_{TBL}$  as very robust, while the value of  $\delta_{TBL}$  depends highly on the definition chosen by the authors and is therefore much more subjective. It should be noted, however, that because heat is transported by conduction within the TBL,  $\delta_{TBL}$  increases with increasing interior temperature and decreasing horizontally averaged surface heat flux.

Alternatively, some previous studies (Vilella & Kaminski, 2017; Vilella & Deschamps, 2018) have suggested to define the TBL using the “hot temperature” profile, that is the

profile composed of the hottest temperature at every depth. More specifically, it has been suggested that the horizontally averaged temperature profile may not be a pertinent choice, since this profile averages the thermal structure of the TBL at different stages of its evolution. It is therefore difficult to use this profile to infer the stability of the TBL or its internal dynamics. On the other hand, when internal heating is dominant, the hot temperature profile captures the thermal structure of the TBL just before it becomes unstable and creates a cold downwelling. As such, the hot temperature profile is particularly appropriate to infer the generation of cold downwellings. In order to quantify the variations induced by the choice of temperature profile, we report in figure S2 the measured value of  $\Delta T_{TBL}$  and  $\delta_{TBL}$  on the horizontally averaged and hot temperature profile, considering the base of the TBL as the point where conduction is negligible. As one can see, there is a systematic difference between the two set of measurements, the TBL in the hot temperature profile being not surprisingly hotter and thinner.

To our knowledge, the previous conclusions are not only valid for these specific cases but for most of convective systems and conditions. As a result, we decided to define the TBL in this present work using the hot temperature profile, to infer the stability of the TBL, and the base of the TBL as the point where conduction is negligible. Note that, as shown by figures S1 and S2, the selection of a different definition should not affect our conclusions, since our reasoning is based on trends rather than on absolute values. An exception, however, is the blue shaded areas displayed in figures S3 and 2. In that case, the thickness of the TBL is highly impacted by the definition we choose. To avoid any potential bias in the decision making process, we have determined the thickness of the TBL at different time-steps using a varieties of definition on both the horizontally averaged

and hot temperature profile. The blue shaded areas account for all these possible values and can therefore be seen as an exhaustive representation of  $\delta_{TBL}$ .

### **Text S2: Effects of the aspect ratio**

The aspect ratio of a numerical simulation is a crucial parameter. If the aspect ratio is too low, the lateral boundaries of the box have a clear impact on the dynamics of the system. In that case, the characteristics and convection planform of the system may be highly impacted by the chosen aspect ratio. By contrast, for an aspect ratio high enough, the characteristics of the system as well as the shape of the convective structures are independent of the chosen aspect ratio. It is therefore vital to select an aspect ratio high enough to avoid any wall-effects.

Traditionally, the aspect ratio is considered as high enough when it involves the generation of a large number of thermal instabilities (at least 10-20). Here, we used this criteria to ensure that our numerical results are robust. This can also be confirmed by observing figures 2 and S3, since there is no significant trade-off between the aspect ratio reported in table 1 and the global characteristics of the convective system. Despite these precautions, one may still question the robustness of our numerical results, especially for  $Ra = 10^7$  where the aspect ratio is varying importantly while being lower than for other cases. To answer this concern, we have conducted an additional numerical simulation with a larger aspect ratio (reported in table S1). These results show that the aspect ratio have a minor impact on the global characteristics of the system. In particular, the differences induced by the aspect ratio are much lower than the differences induced by changing the value of  $d_{HL}$ . As such, our conclusions are unlikely to be impacted by our choice of aspect ratio.

### **Text S3: Interior temperature and heat flux for models with temperature-dependent viscosity and yield stress**

We provide in this paragraph a discussion on the effects of strong viscosity variations and yield stress for a convective system mimicking the Earth’s mantle. For this purpose, we use models of thermal and thermochemical convection performed by Deschamps, Rogister, and Tackley (2018) and Deschamps and Li (2019), together with a few unpublished models. These models were conducted in spherical (Yin-Yang) geometry for a compressible fluids with a rheology including both strong viscosity variations and yield stress. More specifically, the viscosity variations with temperature are controlled by the dimensionless activation energy  $E_a$ . The thermally-induced increase of viscosity is then quantified with a potential thermal viscosity ratio  $\Delta\eta_T = \exp(E_a)$ . However, due to the adiabatic increase of temperature and to the temperature offset, which is fixed to  $T_{off} = 0.88\Delta T_S$ , the effective top-to-bottom thermal viscosity ratio is smaller than  $\Delta\eta_T$  by about two orders of magnitude. Viscosity is further allowed to vary with depth and composition (in thermochemical models). The surface yield stress is assumed to be 290 MPa with a pressure gradient of 0.01. With these values, the yield stress prevents the system from operating in the stagnant lid regime, and all cases are in the mobile lid regime, with surface velocities equivalent to 1 cm/yr or higher. Details of the numerical setups and techniques, e.g., the viscosity law, can be found in these studies. Note that for this setup, the system does not reach a stationary state. However, after a period of time that depends on the values of input parameters, simulations reach a quasi-stationary dynamic, meaning that the top and bottom heat flux and the volume average velocity oscillate around constant values. The values listed in Table S2 are calculated from snapshots taken during the

quasi-stationary stage. Deschamps et al. (2018) do not specify average temperature and heat flux of their models, but we list these data for selected models in Table S2. Note that the temperature fields produced by the numerical code are non-dimensional. The procedure to get dimensional temperatures assumes a surface temperature of 300 K and a super-adiabatic temperature jump of 2500 K, as detailed in the Supplementary Material of Deschamps and Li (2019). Clearly, the results displayed in Table S2 indicate a decrease of the surface heat flux and an increase of the interior temperature as the temperature dependence of viscosity ( $E_a$ ) gets stronger. As a result, the thickness of the top thermal boundary layer, estimated from the ratio between the interior temperature and surface heat flux, increases with increasing temperature-dependence, and is in particular larger for temperature-dependent cases than isoviscous cases.

	$d_{HL}$	Resolution	Aspect ratio	$\phi$	$Ur$	$\Delta T_{TBL}$	$T_{1/2}$	$V_h$	$V_{rms}$
$Ra = 10^7$	0.3	$768 \times 768 \times 192$	4:4:1	$56.17 \pm 0.32$	0.712	0.971	0.721	541	608
$H = 40$	0.3	$768 \times 768 \times 192$	8:8:1	$56.00 \pm 0.19$	0.714	0.991	0.722	538	606

**Table S1.** Input parameters of the numerical simulations: Rayleigh number ( $Ra$ ), dimensionless heating rate ( $H$ ), the thickness of the heat blanket ( $d_{HL}$ ), grid resolution in X:Y:Z directions and the domain aspect ratio in the X:Y:Z directions. We also report some dimensionless characteristics of the system:  $\phi$  the surface heat flux,  $Ur = H/\phi$  the Urey ratio,  $\Delta T_{TBL}$  the temperature jump across the top thermal boundary layer,  $T_{1/2}$  the average temperature at mid-depth,  $V_h$  the average surface velocity,  $V_{rms}$  the volume average root mean square velocity.

$E_a$	$B_z$	$X_{prim}$	pPv	$\langle T \rangle$ (K)	$\Phi_{top}$ (mW/m <sup>2</sup> )	Reference
0.0	-	-	no	1320	125.8	Unpublished
13.816	-	-	no	2030	75.0	Deschamps et al. (2018), model T2
18.421	-	-	no	2220	57.9	Unpublished
20.723	-	-	no	2280	53.6	Deschamps et al. (2018), model T1
23.026	-	-	no	2300	56.5	Deschamps et al. (2018), model T3
13.816	-	-	yes	2280	96.4	Deschamps et al. (2018), model T2-pPv
20.723	-	-	yes	2490	80.4	Deschamps et al. (2018), model T1-pPv
0.0	0.15	3.5	no	950	60.6	Unpublished
13.816	0.15	3.5	no	1620	42.6	Unpublished
20.723	0.15	3.5	no	1970	35.0	Deschamps et al. (2018), model TC4
0.0	0.23	3.5	no	930	60.7	Unpublished
13.816	0.23	3.5	no	1470	43.4	Deschamps et al. (2018), model TC2
18.421	0.23	3.5	no	1720	35.4	Unpublished
20.723	0.23	3.5	no	1900	34.1	Deschamps et al. (2018), model TC1
23.026	0.23	3.5	no	1970	30.6	Deschamps et al. (2018), model TC3
13.816	0.23	3.5	yes	1840	56.5	Deschamps et al. (2018), model TC2-pPv
20.723	0.23	3.5	yes	2160	48.5	Deschamps et al. (2018), model TC1-pPv

**Table S2.** Average interior temperature,  $\langle T \rangle$ , and surface heat flux,  $\Phi_{top}$ , for selected thermal and thermo-chemical models. Viscosity variations with temperature are controlled by the parameter  $E_a$ . For thermo-chemical models, the buoyancy ratio,  $B_z$ , and volume fraction of dense material,  $X_{prim}$ , are listed. All models include yield stress, and 4 models also include post-perovskite (pPv) lenses at the bottom of the shell.

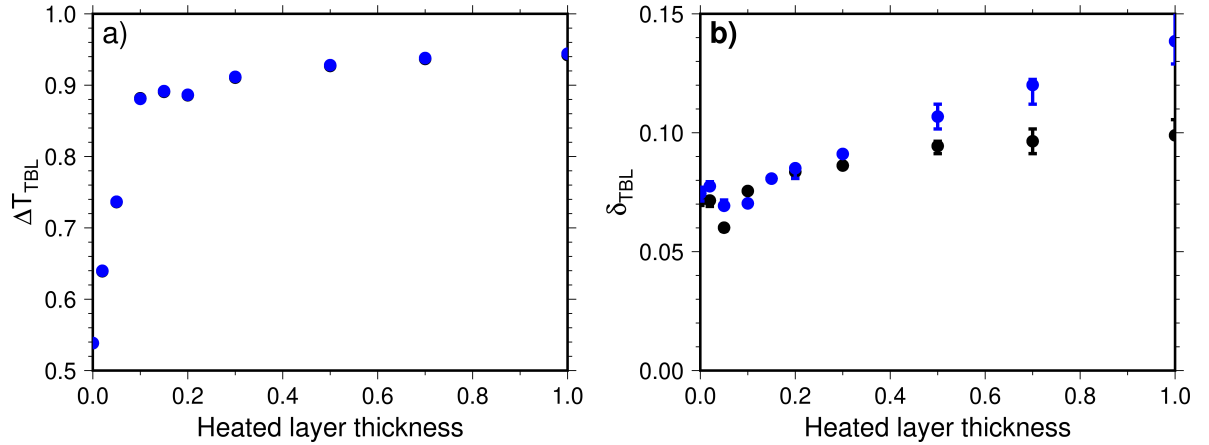


**Figure S1.** Variations of the dimensionless (a) temperature jump across the top thermal boundary layer ( $\Delta T_{TBL}$ ) and (b) thickness of the top thermal boundary layer as a function of the dimensionless thickness of the heat blanket ( $d_{HL}$ ). The numerical simulations are conducted for  $Ra = 10^6$  and  $H = 20$ . The base of the thermal boundary layer is either defined as the point where conduction is negligible (black symbols) or the point where the temperature is locally maximum (blue symbols). Note that the two set of data points are superimposed for  $\Delta T_{TBL}$ . Error bars correspond to temporal variation (smaller than the symbol size for  $\Delta T_{TBL}$ ).

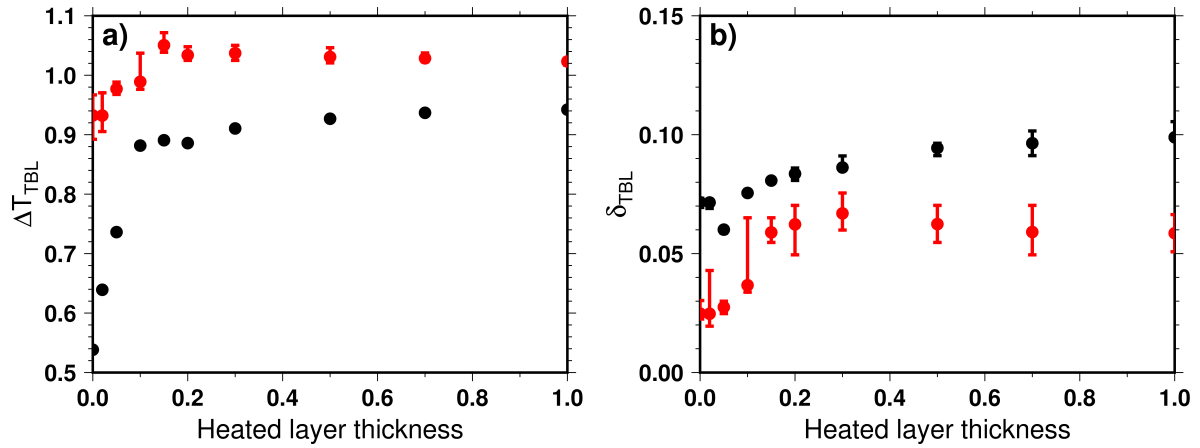


**Figure S2.** Variations of the dimensionless (a) temperature jump across the top thermal boundary layer ( $\Delta T_{TBL}$ ) and (b) thickness of the top thermal boundary layer as a function of the dimensionless thickness of the heat blanket ( $d_{HL}$ ). The numerical simulations are conducted for  $Ra = 10^6$  and  $H = 20$ . The base of the thermal boundary layer defined as the point where conduction is negligible on either the horizontally averaged profile (black symbols) or the “hot temperature” profile (red symbols). Error bars correspond to temporal variation.

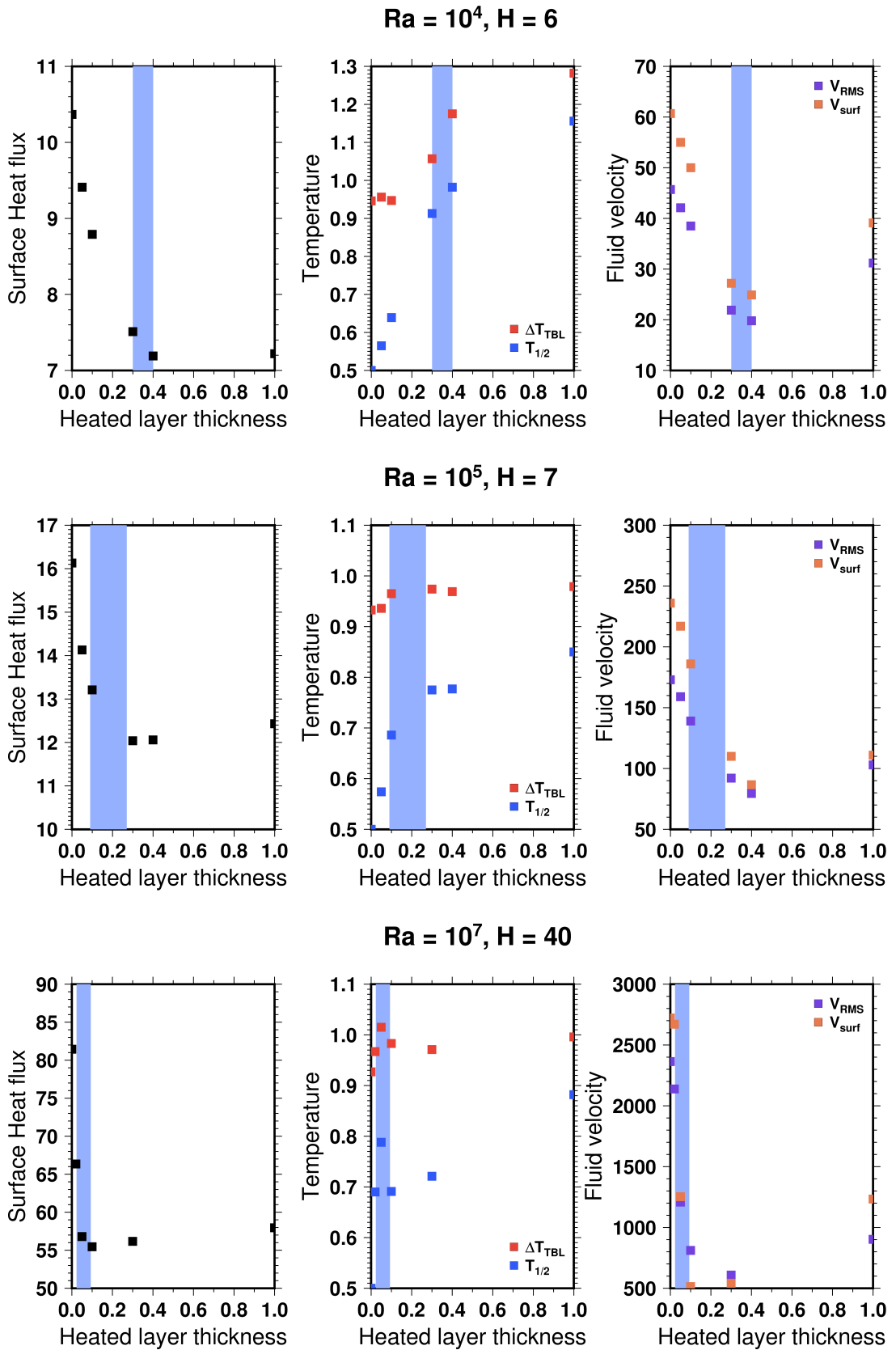
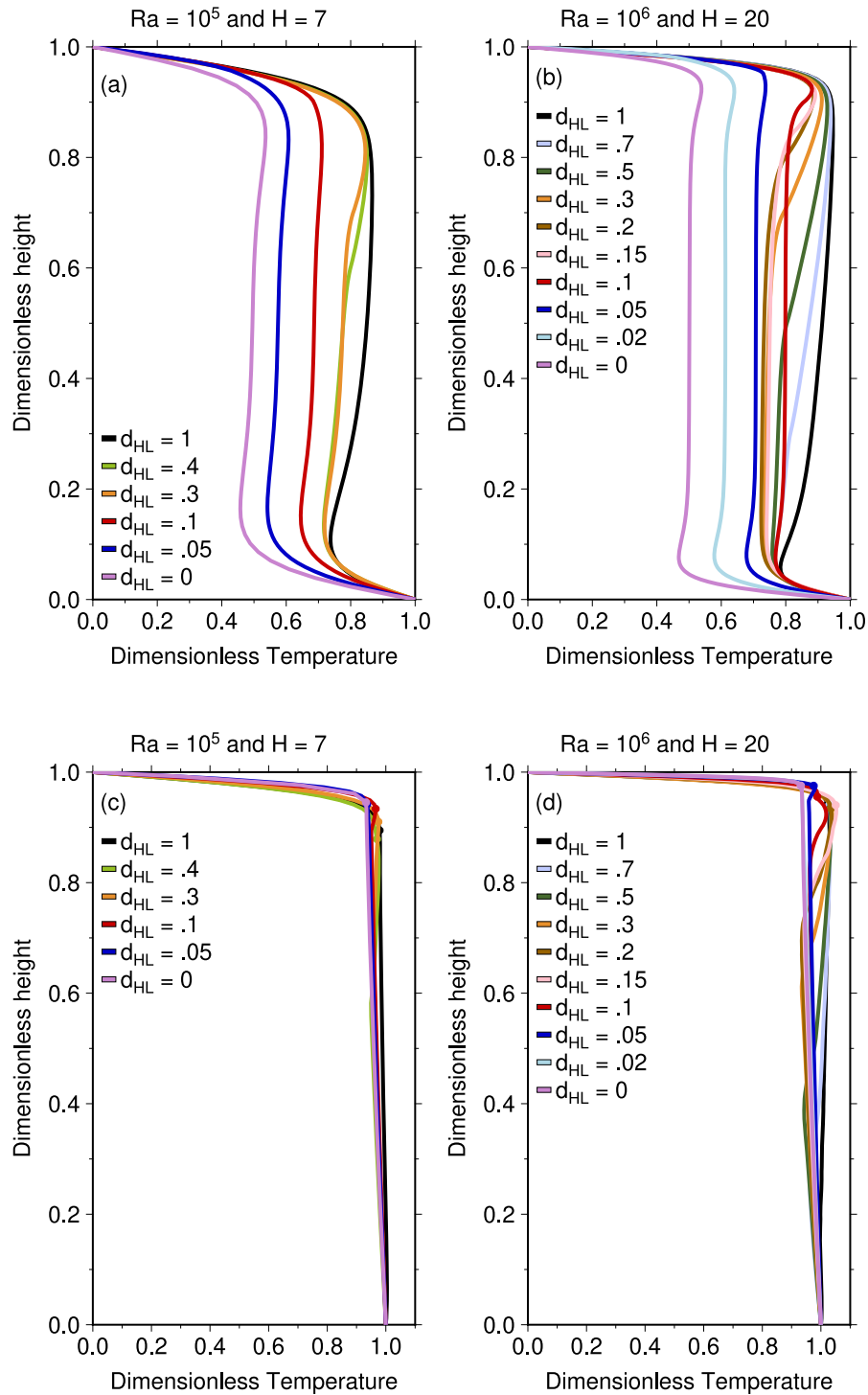


Figure S3. See caption of figure 2.



**Figure S4.** Horizontally averaged temperature profiles (top panels) and “hot” temperature profiles (bottom panels) for numerical simulations conducted with (a, c)  $Ra = 10^5$  with  $H = 7$  and (b, d)  $Ra = 10^6$  with  $H = 20$ . “Hot” temperature profiles are built from the hottest temperature at a given depth. The base of the thermal boundary layer determined by the method presented in text S1 is indicated with a circle.

## References

- Deschamps, F., & Li, Y. (2019). Core-Mantle Boundary Dynamic Topography: Influence of Postperovskite Viscosity. *Journal of Geophysical Research: Solid Earth*, *124*, 9247–9264. doi: 10.1029/2019JB017859
- Deschamps, F., Rogister, Y., & Tackley, P. J. (2018). Constraints on core-mantle boundary topography from models of thermal and thermo-chemical convection. *Geophysical Journal International*, *212*, 164–188. doi: 10.1093/gji/ggx402
- Parmentier, E. M., & Sotin, C. (2000). Three-dimensional numerical experiments on thermal convection in a very viscous fluid: Implications for the dynamics of a thermal boundary layer at high Rayleigh number. *Physics of Fluids*, *12*, 609–617. doi: 10.1063/1.870267
- Sotin, C., & Labrosse, S. (1999). Three-dimensional thermal convection in an iso-viscous, infinite Prandtl number fluid heated from within and from below: applications to the transfer of heat through planetary mantles. *Physics of the Earth and Planetary Interiors*, *112*, 171–190. doi: 10.1016/S0031-9201(99)00004-7
- Vilella, K., & Deschamps, F. (2018). Temperature and heat flux scaling laws for isoviscous, infinite Prandtl number mixed heating convection. *Geophysical Journal International*, *214*, 265–281. doi: 10.1093/gji/ggy138
- Vilella, K., & Kaminski, E. (2017). Fully determined scaling laws for volumetrically heated convective systems, a tool for assessing habitability of exoplanets. *Physics of the Earth and Planetary Interiors*, *266*, 18–28. doi: 10.1016/j.pepi.2017.02.001